

Supporting Information

Structural Basis for Inhibition of ROS-Producing Respiratory Complex I by NADH-OH

Marta Vranas, Daniel Wohlwend, Danye Qiu, Stefan Gerhardt, Christian Trncik, Mehrosh Pervaiz, Kevin Ritter, Stefan Steimle, Antonio Randazzo, Oliver Einsle, Stefan Günther, Henning J. Jessen, Alexander Kotlyar, and Thorsten Friedrich**

anie_202112165_sm_miscellaneous_information.pdf

Supporting Information

Contents

Supporting Materials and Methods

Preparation of NuoEF

Preparation of NADH-OH

Protein crystallization

Structure analysis

Alignment of sequences from human proteins containing a Rossmann-fold

Data availability

Supporting Figures (S1 - S6)

Supporting Tables (S1 - S2)

Supporting References

Supporting Materials and Methods

Preparation of NuoEF

A. aeolicus NuoEF was isolated from an overproducing *E. coli* strain by anion-exchange chromatography on Source 15Q material, affinity chromatography on Ni²⁺-IDA material and size-exclusion chromatography on TSKgel G4000SW in a 50 mM MOPS/NaOH, 50 mM NaCl buffer at pH 7.0.^[14]

Preparation of NADH-OH

The inhibitor was produced during incubation of NADH in an oxygen-saturated 50% ethanol solution containing 0.1 M NaOH at room temperature for 2 days and purified from non-modified NADH, products of its degradation and other NADH derivatives co-produced with NADH-OH by ion-exchange chromatography essentially as described.^[12] The inhibitor obtained using the above procedure is still strongly contaminated by nucleotide derivatives. In order to completely purify NADH-OH the following approach has been used. NuoEF was mixed with partly purified (by chromatography) NADH-OH. The affinity of the enzyme to NADH-OH is much higher than to other dinucleotide derivatives present in the inhibitor preparation, leading to selective binding of only NADH-OH to the enzyme (Figure S1A). The impurities were separated from the enzyme-inhibitor complex by ultrafiltration (Figure S1B). Three to four ultrafiltration steps lead to complete purification of the complex from low molecular weight contaminants (oligonucleotide and di- and mono-nucleotide derivatives). The absorption spectrum of the purified enzyme-inhibitor complex was recorded and compared to that of the untreated NuoEF. The inhibitor was dissociated from NuoEF at pH 11 and separated from the enzyme by ultrafiltration (Figure S1C). NADH-OH is very stable at alkaline pH^[10-12] in contrast to the enzyme which undergoes irreversible denaturation. We have shown that the absorption spectrum of the inhibitor fraction is identical to that of the initial NADH-OH. We thus conclude that no irreversible changes (oxidation) of the inhibitor took place in the active center of the enzyme.

Protein crystallization

The preparation of NuoEF was crystallized at 20°C by sitting drop vapor diffusion containing 0.1 M Tris/HCl and 1.0 M sodium citrate, pH 6.9-7.1 as precipitant.^[14] Each well contained equal molar concentrations of NuoEF and NADH-OH. The crystals were transferred to a 1:1 (v/v) mixture of paratone N / paraffin oil before flash-freezing into liquid nitrogen.

Structure analyses

Diffraction data of the original NuoEF with bound NADH-OH were collected at beamline X06SA at the Swiss Light Source (Villigen, Switzerland). Crystals were exposed to the X-ray beam at cryogenic temperatures (100 K). The crystal structure in complex with NADH-OH was solved by molecular replacement with the native structure^[14] as the search model. Table S1 summarizes the statistics for crystallographic data collection and structural refinement. The structure was refined to convergence applying non-crystallographic symmetry in all subsequent rounds of positional refinement using local structure similarity restraints (LSSR) including TLS as implemented in the program autoBuster.^[20,21] X-ray diffraction intensities were processed using XDS and further scaled and analyzed using AIMLESS as implemented in autoProc tool box.^[22] Stereochemical ligand restraints of NADH-OH were generated using WRITEDICT and coordinates subsequently placed into 2F_o-F_c electron density maps using the AFITT-CL program (version 2.4.0.4, OpenEye Scientific Software, Inc., Santa Fe, NM, USA) (AFITT 2.4.0.4: OpenEye Scientific Software, Inc., Santa Fe, NM, USA. <http://www.eyesopen.com/>).^[23]

Alignment of sequences from human proteins containing a Rossmann-fold

Structures of human NAD(P)(H)-binding proteins with Rossmann fold domain, as classified by SCOP,^[24] were retrieved from the PDB. Redundant sequences were removed using a 95% identity criteria by CD-Hit.^[25] The alignment was built using the structural alignment tool Expresso.^[26] ClustalW^[27] and T-coffee^[28] multiple sequence alignments were used for library computation and templates were automatically fetched from the PDB. All other parameters used were kept default. Jalview^[29] was used to visualise the alignment.

Data availability:

Coordinates have been deposited under the PDB entry 6SAQ.

Supporting Information

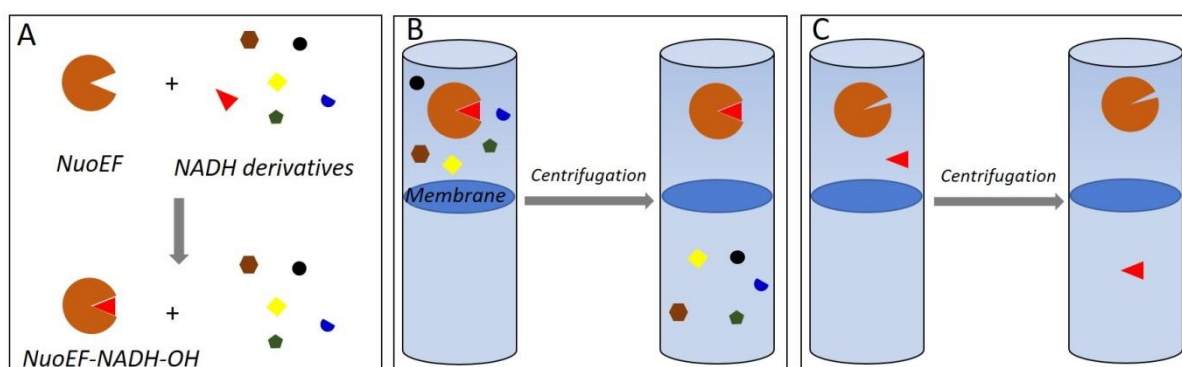


Figure S1. Scheme of purification of NADH-OH. (A) Selective binding of the inhibitor (red triangle) by a NuoEF molecule (red). The other unknown nucleotide components contained within the reaction mixture are represented as other symbols with different colors. (B) Separation of a NuoEF-NADH-OH complex from non-bound dinucleotide derivatives (colored shapes) by ultrafiltration. (C) Dissociation of the inhibitor from the active center of NuoEF at alkaline pH and separation from the denatured enzyme by ultrafiltration.

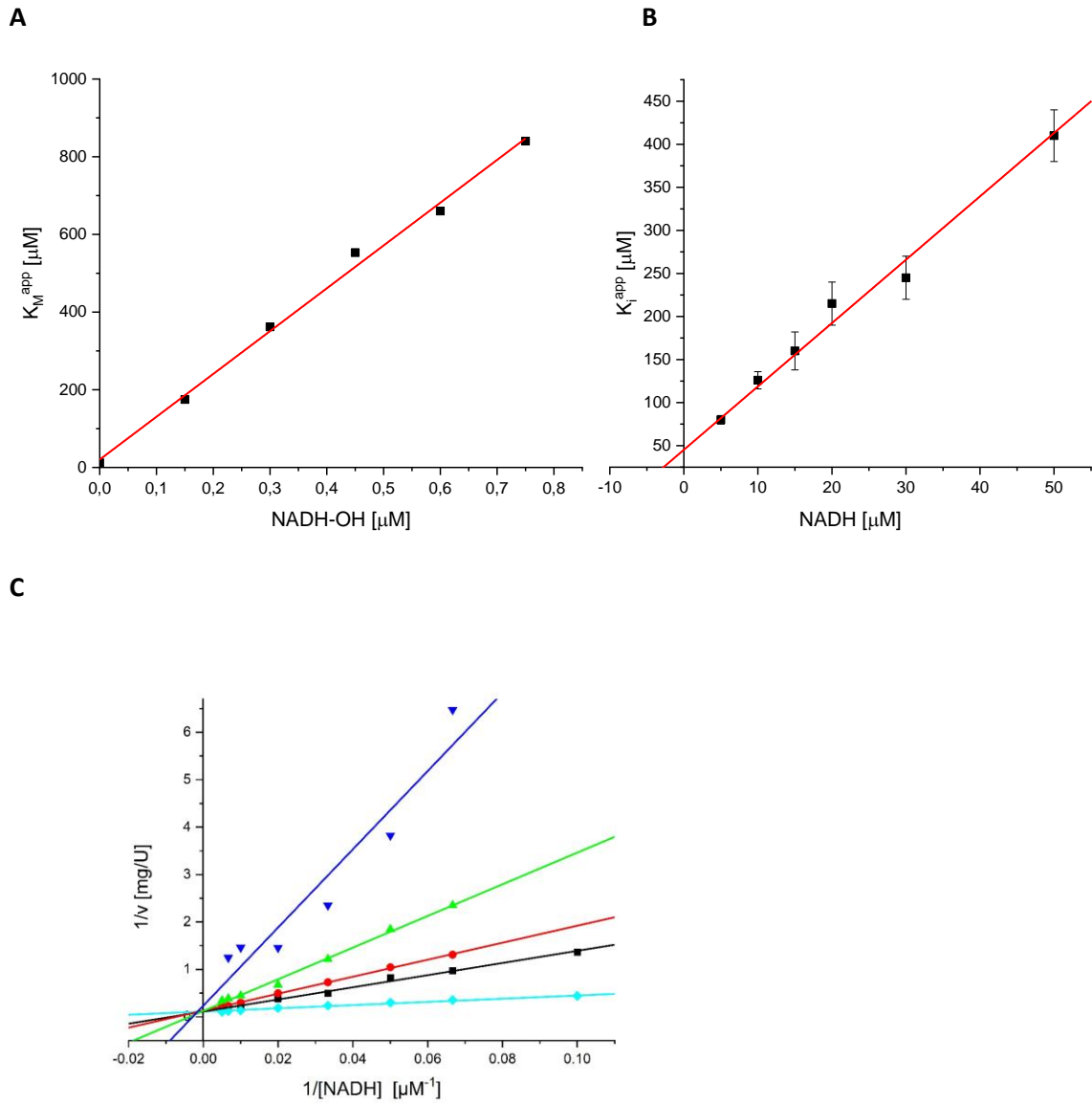
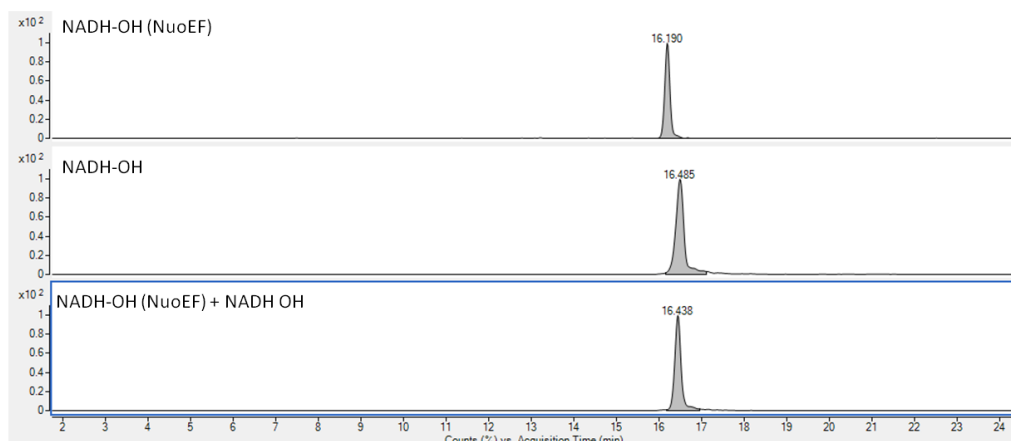


Figure S2. Inhibition of bovine heart (A) and *E. coli* (B, C) complex I by NADH-OH. NADH-OH purified by binding to NuoEF was used throughout. (A) NADH oxidase activity of bovine heart mitochondria^[30] were assayed in 100 mM K-Pi, 100 μ M EDTA, pH 7.4, by following the decrease of absorbance at 340 nm. The apparent K_m to NADH was determined from Lineweaver-Burk plots at constant NADH-OH concentrations. The K_m towards NADH in the absence of NADH-OH was 12 μ M. The plot reflects the best fit for $K_m(app) = (K_m + [NADH-OH]/K_i)$ with K_i being 10 nM. (B) Due to the high affinity of NADH-OH to *E. coli* complex I, the K_i was calculated according to:^[31]

$$I_i / (1 - (v_i/v_o)) = K_i (S_t + K_m/K_m) (v_o/v_i) + E_t$$

The plot resulted in a K_i of 46 nM. (C) Lineweaver-Burk plots of reciprocals of the reaction rate versus the NADH concentration at various NADH-OH concentrations: 0 μ M (cyan), 0.2 μ M (black), 0.5 μ M (red), 0.8 μ M (green), and 2.0 μ M (blue). The intersection of the regression lines at $x=0$ indicates a competitive inhibition. Note, a slight shift from the intersection point into the second quadrant is observed for the titration at 2.0 μ M NADH-OH (blue).

A)



B)

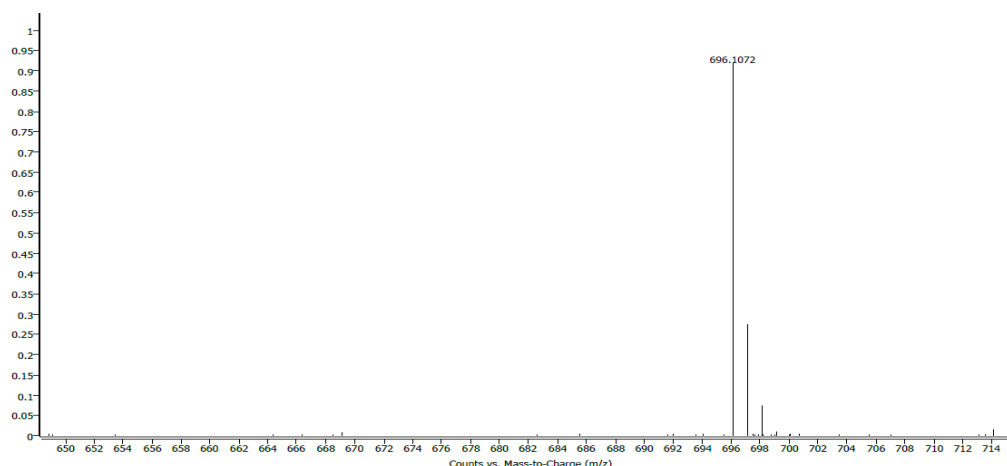


Figure S3. CE-ESI-MS analysis of NADH-OH. A) NADH-OH bound to and released from NuoEF (NADH-OH (NuoEF)) and NADH-OH prepared by chromatographic methods were injected into a CE-column and eluted after the same retention time. The two samples were mixed, injected and eluted as a single peak at the same retention time. All three runs resulted in the same MS spectrum (Expected mass: 696.107, found mass: 696.107) shown in B) demonstrating that NADH-OH that was purified by chromatographic methods and NADH-OH bound to NuoEF are identical compounds.

CE-ESI-MS measurements were performed on a bare-fused silica capillary with a length of 100 cm (50 μ m internal diameter and 365 μ m outer diameter) on an Agilent 7100 capillary electrophoresis system coupled to a Q-TOF mass analyzer (6545, Agilent) equipped with electrospray ionization (ESI) source. CE-MS sheath flow interface containing an adapter and sprayer kit were from Agilent. 35 mM ammonium acetate titrated by ammonia solution to pH 9.7 was employed as CE running buffer. Samples were introduced at 100 mbar pressure for 10 s. The separation voltage was set to 30 kV. The sheath liquid composed of a water-isopropanol (1:1) mixture spiked with mass references was introduced at a constant flow rate of 6 μ L/min. ESI-TOF-MS was conducted in the negative ionization mode; the capillary voltage was set to -3500 V. The fragmentor, skimmer, and Oct RFV voltage was set to 100, 60, and 750 V, respectively. The temperature and flow rate of drying gas was 250 $^{\circ}$ C and 3 L/min, respectively. Nebulizer gas pressure was 11 psi. Peak assignment of NADH-OH is according to the accurate mass to charge ratio.

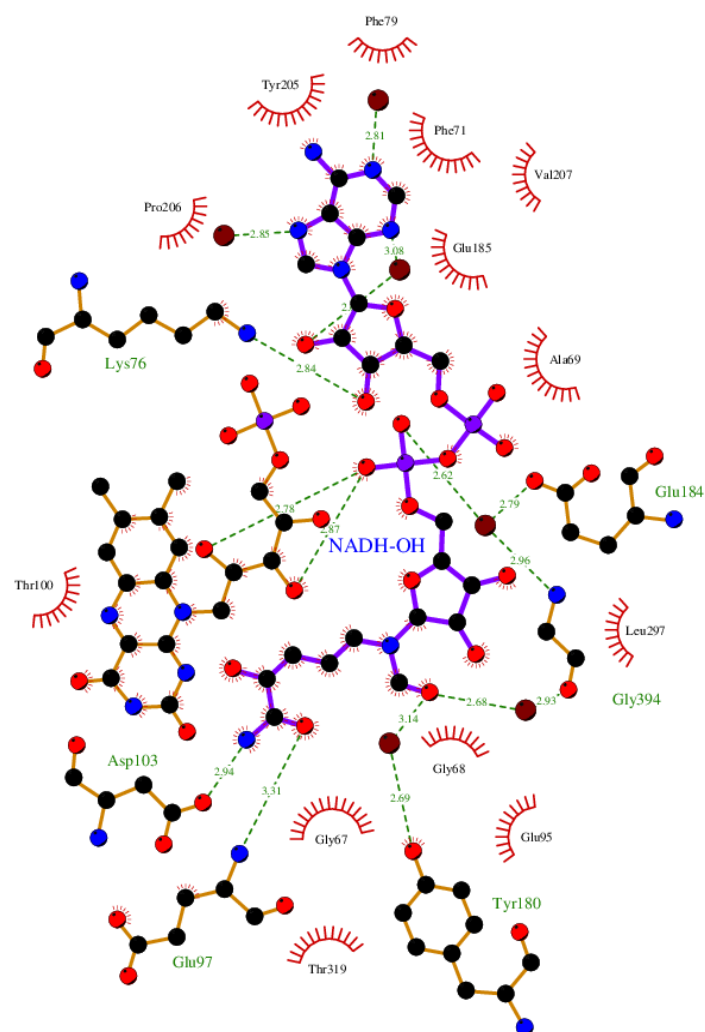


Figure S4. Interactions of NADH-OH with the Rossmann-fold of NuoF. The numbering of the amino acid positions refers to the *A. aeolicus* enzyme. Note that the orientation of this figure is turned by 180° compared to Fig. 3 of the main text.

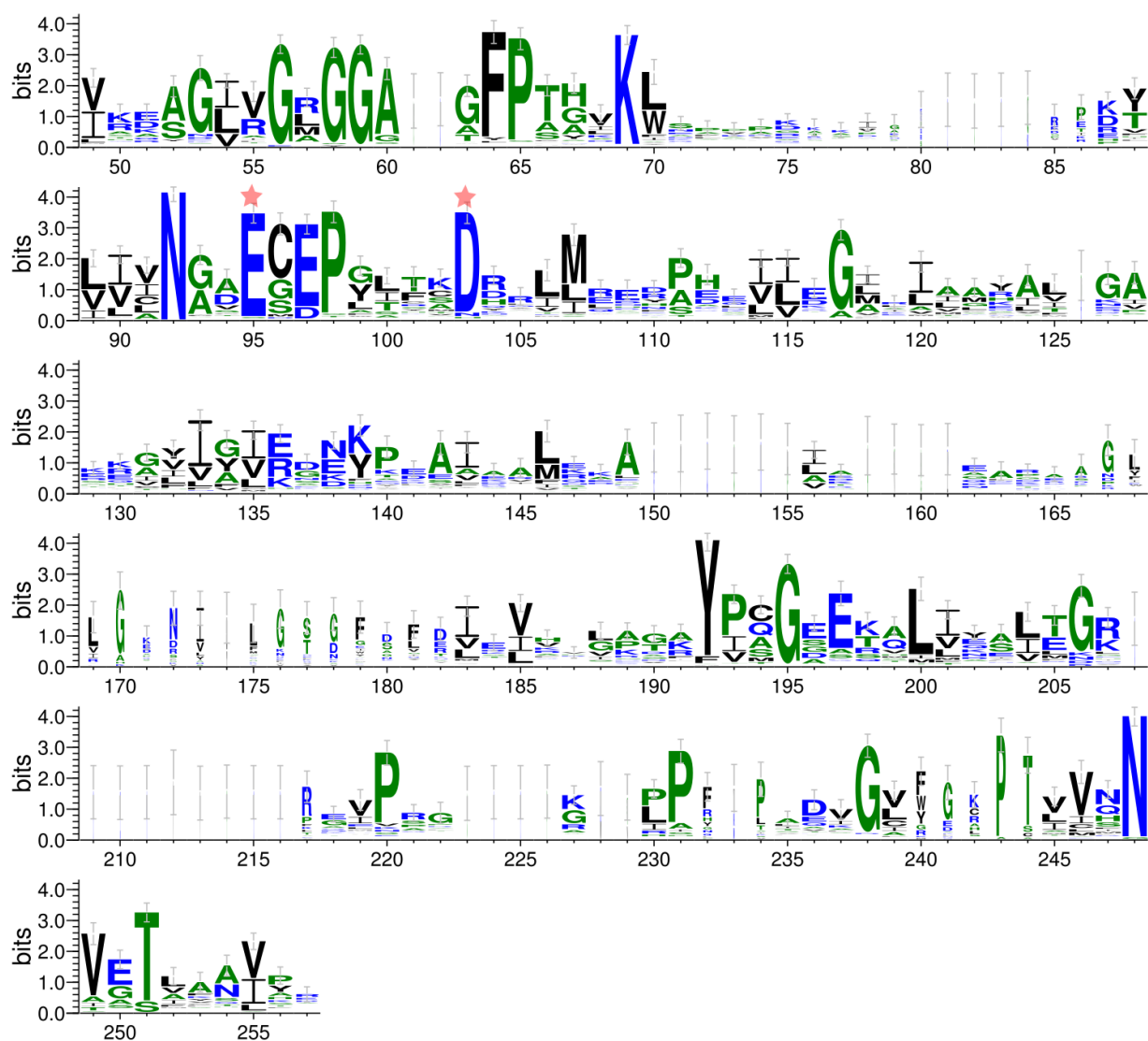


Figure S5. Sequence conservation of complex I subunit NuoF across different species. The sequence logo^[32] was generated for the Pfam^[33] seed alignment of the complex I 51 kDa subunit family (PF01512) using the tool WebLogo^[34]. Residues E95 and D103 are highlighted with stars. The x-axis corresponds to residue positions in the NuoF sequence.

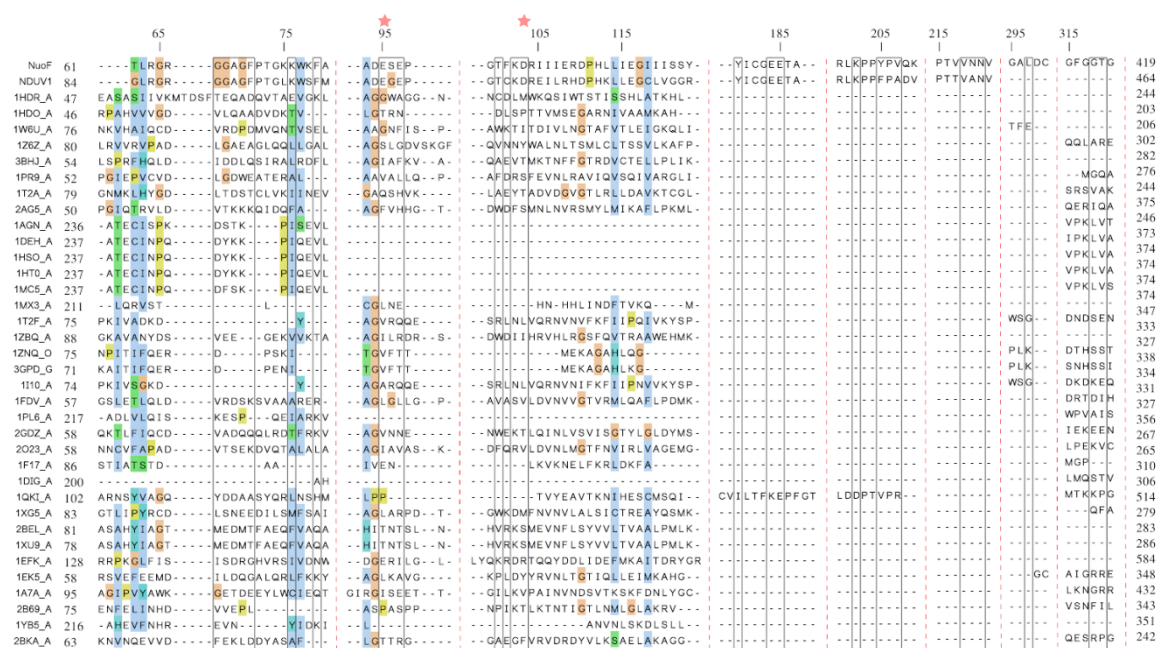


Figure S6. Structure-based sequence alignment of NuoF and human NAD-binding proteins with a Rossmann fold domain. Residues that make up the NuoF binding site are enclosed within vertical boxes. The residues E95 and D103 are highlighted with stars. Only parts of the alignment are shown. The vertical dashed lines show the positions where the alignment was cut. PDB identifiers for each sequence are shown on the left (except for NuoF and its human counterpart (NDUV1)). Numbers on the left represent the first residue that is shown and numbers on the right represent the complete length of each aligned sequence. The numbers at the top of the alignment correspond to the unaligned NuoF sequence and are shown only for comparison.

Table S1. Data collection and refinement statistics.

Data Set	NADHOH
space group	$P2_1$
wavelength [Å]	1.000020
cell constants a, b, c [Å]	96.0, 63.8, 121.4
α, β, γ [°]	90.0, 105.7, 90.0
resolution limits [Å]	116.9 – 2.02 (2.13 – 2.02)
completeness (%)	99.9 (99.9)
unique reflections	92,408 (13,438)
multiplicity (%)	3.8 (3.8)
$R_{\text{merge}}^{\text{a)}}$	0.072 (0.515)
$R_{\text{p.i.m.}}$	0.050 (0.352)
mean $I / \sigma(I)$	11.4 (2.5)
$CC_{1/2}$	0.997 (0.741)
refinement statistics	
$R_{\text{cryst}}^{\text{b)}}$	0.159
R_{free} (%)	0.181
non-hydrogen atoms	9124
solvent molecules	605
r.m.s. deviations from ideal values	
bond lengths (Å)	0.010
bond angles (°)	0.96
average B values (Å²)	
protein main chain atoms	33.9
protein all atoms	37.3
FMN	22.5
NADOH	28.8
FES	26.2
SF4	26.0
solvent	45.7
Wilson plot	32.2
Φ, Ψ angle distribution	
Residues in most favoured regions	92.0
in additional allowed regions	7.6
in generously allowed regions	0.2
in disallowed regions	0.2

$$^{\text{a}} R_{\text{merge}} = \sum_{hkl} [(\sum_i |I_i - \langle I \rangle|) / \sum_i I_i]$$

$$^{\text{b}} R_{\text{cryst}} = \sum_{hkl} ||F_{\text{obs}}| - |F_{\text{calc}}|| / \sum_{hkl} |F_{\text{obs}}|$$

R_{free} is the cross-validation R value for a test set of 5 % of unique reflections.

Table S2. List of putative mitochondrial dioxygenases. All proteins are from MitoCarta 2.0^[35] and are related to proteins from EC classes 1.13.*.* or 1.14.*.* containing dioxygenases.

SYM	SYNONYMS	DESCRIPTION
COQ7	CAT5 CLK-1 CLK1 Q99807	coenzyme Q7 homolog, ubiquinone (yeast)
UQCRFS1	RIP1 RIS1 RISP UQCR5 P47985	ubiquinol-cytochrome c reductase, Rieske iron-sulfur polypeptide 1
ECHS1	SCEH P30084	enoyl CoA hydratase, short chain, 1, mitochondrial
HADHA	ECHA GBP HADH LCEH LCHAD MTPA TP-ALPHA P40939	hydroxyacyl-CoA dehydrogenase/3-ketoacyl-CoA thiolase/enoyl-CoA hydratase (trifunctional protein), alpha subunit
ACADS	ACAD3 SCAD P16219	acyl-CoA dehydrogenase, C-2 to C-3 short chain
AUH	Q13825	AU RNA binding protein/enoyl-CoA hydratase
COQ6	CGI10 COQ10D6 Q9Y2Z9	coenzyme Q6 monooxygenase
ECHDC3	Q96DC8	enoyl CoA hydratase domain containing 3
ACADM	ACAD1 MCAD MCADH P11310	acyl-CoA dehydrogenase, C-4 to C-12 straight chain
SUPV3L1	SUV3 Q8IYB8	suppressor of var1, 3-like 1 (S. cerevisiae)
ACADL	ACAD4 LCAD P28330	acyl-CoA dehydrogenase, long chain
FDX1	ADX FDX LOH11CR1D P10109	ferredoxin 1
ECH1	HPXEL Q13011	enoyl CoA hydratase 1, peroxisomal
ERAL1	ERA ERAL1A H-ERA HERA-A HERA-B O75616	Era-like 12S mitochondrial rRNA chaperone 1
ACADSB	2-MEBCAD ACAD7 SBCAD P45954	acyl-CoA dehydrogenase, short/branched chain
ACADVL	ACAD6 LCACD VLCAD P49748	acyl-CoA dehydrogenase, very long chain
ECHDC2	Q86YB7	enoyl CoA hydratase domain containing 2
ACAD8	ACAD-8 ARC42 Q9UKU7	acyl-CoA dehydrogenase family, member 8
IVD	ACAD2 P26440	isovaleryl-CoA dehydrogenase
L2HGDH	C14orf160 Q9H9P8	L-2-hydroxyglutarate dehydrogenase
ETHE1	HSCO YF13H12 O95571	ethylmalonic encephalopathy 1
GCDH	ACAD5 GCD Q92947	glutaryl-CoA dehydrogenase
HAGH	GLO2 GLX2 GLXII HAGH1 Q16775	hydroxyacylglutathione hydrolase
MTG1	GTP GTPBP7 RP11-108K14.2 Q9BT17	mitochondrial ribosome-associated GTPase 1
GPD2	GDH2 GPDM mGPDH P43304	glycerol-3-phosphate dehydrogenase 2 (mitochondrial)
SLC25A25	MCSC PCSC RP11-395P17.4 SCAMC-2 Q6KCM7	solute carrier family 25 (mitochondrial carrier; phosphate carrier), member 25
ACAD10	Q6JQN1	acyl-CoA dehydrogenase family, member 10
ALKBH7	ABH7 SPATA11 UNQ6002 Q9BT30	alkB, alkylation repair homolog 7 (E. coli)

ECI2	ACBD2 DRS-1 DRS1 HCA88 PECI dJ1013A10.3 O75521	enoyl-CoA delta isomerase 2
MCEE	GLOD2 Q96PE7	methylmalonyl CoA epimerase
OXNAD1	Q96HP4	oxidoreductase NAD-binding domain containing 1
MTG2	GTPBP5 ObgH1 dJ1005F21.2 Q9H4K7	mitochondrial ribosome-associated GTPase 2
FDX1L	FDX2 Q6P4F2	ferredoxin 1-like
EHHADH	ECHD FRTS3 L-PBE LBFP LBP PBFE Q08426	enoyl-CoA, hydratase/3-hydroxyacyl CoA dehydrogenase
ACAD9	NPD002 Q9H845	acyl-CoA dehydrogenase family, member 9
SUOX	P51687	sulfite oxidase
SARDH	BPR-2 DMGDHL1 SAR SARD SDH Q9UL12	sarcosine dehydrogenase
SLC25A24	APC1 SCAMC-1 Q6NUK1	solute carrier family 25 (mitochondrial carrier; phosphate carrier), member 24
NOA1	C4orf14 MTG3 hAtNOS1 hNOA1 mAtNOS1 Q8NC60	nitric oxide associated 1
ECI1	DCI P42126	enoyl-CoA delta isomerase 1
ECHDC1	HEL-S-76 MMCD dJ351K20.2 Q9NTX5	enoyl CoA hydratase domain containing 1
LACTB2	Q53H82	lactamase, beta 2
HAO2	GIG16 HAOX2 Q9NYQ3	hydroxyacid oxidase 2 (long chain)
PDPR	PDP3 Q8NCN5	pyruvate dehydrogenase phosphatase regulatory subunit
GTPBP3	GTPBG3 MSS1 MTGP1 THDF1 Q969Y2	GTP binding protein 3 (mitochondrial)
PPOX	PPO V290M VP P50336	protoporphyrinogen oxidase
ACAD11	ACAD-11 Q709F0	acyl-CoA dehydrogenase family, member 11
DMGDH	DMGDHD ME2GLYDH Q9UI17	dimethylglycine dehydrogenase
TOMM70A	O94826	translocase of outer mitochondrial membrane 70 homolog A (S. cerevisiae)
CYP27A1	CP27 CTX CYP27 Q02318	cytochrome P450, family 27, subfamily A, polypeptide 1
KMO	dJ317G22.1 O15229	kynurenine 3-monooxygenase (kynurenine 3-hydroxylase)
ELAC2	COXPD17 ELC2 HPC2 Q9BQ52	elaC ribonuclease Z 2
SLC25A23	APC2 MCSC2 SCaMC-3 Q9BV35	solute carrier family 25 (mitochondrial carrier; phosphate carrier), member 23
PHYH	LN1 LNAP1 PAHX PHYH1 RD O14832	phytanoyl-CoA 2-hydroxylase
CYB5B	CYB5-M CYPB5M OMB5 RP11-140H17.1 O43169	cytochrome b5 type B (outer mitochondrial membrane)
PNPO	HEL-S-302 PDXPO Q9NVS9	pyridoxamine 5'-phosphate oxidase
AIFM3	AIFL Q96NN9	apoptosis-inducing factor, mitochondrion-associated, 3
ALKBH3	ABH3 DEPC-1 DEPC1 PCA1 Q96Q83	alkB, alkylation repair homolog 3 (E. coli)

RECQL4	RECQ4 O94761	RecQ protein-like 4
GTPBP10	ObgH2 A4D1E9	GTP-binding protein 10 (putative)
CYB5A	CYB5 MCB5 P00167	cytochrome b5 type A (microsomal)
PTPN4	MEG PTPMEG PTPMEG1 P29074	protein tyrosine phosphatase, non-receptor type 4 (megakaryocyte)
SYNJ2BP	ARIP2 OMP25 P57105	synaptojanin 2 binding protein
MAOB	P27338	monoamine oxidase B
CYB5R3	B5R DIA1 P00387	cytochrome b5 reductase 3
DDX28	MDDX28 Q9NUL7	DEAD (Asp-Glu-Ala-Asp) box polypeptide 28
GTPBP6	PGPL O43824	GTP binding protein 6 (putative)
CYP11A1	CYP11A CYPXIA1 P450SCC P05108	cytochrome P450, family 11, subfamily A, polypeptide 1
NLRX1	CLR11.3 DLNB26 NOD26 NOD5 NOD9 Q86UT6	NLR family member X1
FOXRED1	H17 Q96CU9	FAD-dependent oxidoreductase domain containing 1
FBXL4	FBL4 FBL5 MTDPS13 Q9UKA2	F-box and leucine-rich repeat protein 4
MAOA	MAO-A P21397	monoamine oxidase A
TMLHE	AUTSX6 BBOX2 TMLD TMLH TMLHED XAP130 Q9NVH6	trimethyllysine hydroxylase, epsilon
KIF1B	CMT2 CMT2A CMT2A1 HMSNII KLP NBLST1 O60333	kinesin family member 1B
DHX30	DDX30 RETCOR Q7L2E3	DEAH (Asp-Glu-Ala-His) box helicase 30
CYP24A1	CP24 CYP24 HCAI P450-CC24 Q07973	cytochrome P450, family 24, subfamily A, polypeptide 1
CYP11B2	ALDOS CPN2 CYP11B CYP11BL CYPXIB2 P-450C18 P450C18 P450aldo P19099	cytochrome P450, family 11, subfamily B, polypeptide 2
CYP27B1	CP2B CYP1 CYP1alpha CYP27B P450c1 PD DR VDD1 VDDR VDDR1 VDR O15528	cytochrome P450, family 27, subfamily B, polypeptide 1
EFHD1	MST133 MSTP133 SWS2 Q9BUP0	EF-hand domain family, member D1
CYB5R2	B5R.2 Q6BCY4	cytochrome b5 reductase 2
NUCB2	HEL-S-109 NEFA P80303	nucleobindin 2
ALKBH1	ABH ABH1 ALKBH alkB hABH Q13686	alkB, alkylation repair homolog 1 (E. coli)

References

- [20] G. Bricogne, E. Blanc, M. Brandl, C. Flensburg, P. Keller, W. Paciorek, P. Roversi, A. Sharff, O. S. Smart, C. Vonrhein, T. O. Womack, **2011**, BUSTER version 2.10.2. Cambridge, UK, Global Phasing Ltd.
- [21]. O. S. Smart, T. O. Womack, C. Flensburg, P. Keller, W. Paciorek, A. Sharff, C. Vonrhein, G. Bricogne, *Acta Cryst. D* **2012**, *68*, 368-380.
- [22] C. Vonrhein, C. Flensburg, P. Keller, A. Sharff, O. S. Smart, W. Paciorek, T. O. Womack, G. Bricogne, *Acta Cryst. D* **2011**, *67*, 293-302.
- [23] S. Wlodek, A. G. Skillman, A. Nicholls, *Acta Cryst. D* **2006**, *62*, 741-749.
- [24] A. G. Murzin, S. E. Brenner, T. Hubbard, C. Chothia, *J. Mol. Biol.* **1995**, *247*, 536-540.
- [25] W. Li, A. Godzik, *Bioinformatics* **2006**, *22*, 1658-1659.
- [26] F. Armougom, S. Moretti, O. Poirot, S. Audic, P. Dumas, B. Schaeli, V. Keduas, C. Notredame, *Nucl. Acids Res.* **2006**, *34*, W604-608.
- [27] M. A. Larkin, G. Blackshields, N. P. Brown, R. Chenna, P. A. McGettigan, H. McWilliam, F. Valentin, I. M. Wallace, A. Wilm, R. Lopez, J. D. Thompson, T. J. Gibson, D. Higgins, *Bioinformatics*. **2007**, *23*, 2947-2948.
- [28] C. Notredame, D. G. Higgins, J. T. Heringa, *J. Mol. Biol.* **2000**, *302*, 205-217.
- [29] A.M. Waterhouse, J. B. Procter, D. M. Martin, *Bioinformatics* **2009**, *25*, 1189-1191.
- [30] V. G. Grivennikova, A. D. Vinogradov, *Biochim. Biophys. Acta* **2013**, *1827*, 446-454.
- [31] P. J. Henderson, *Biochem. J.* **1927**, *127*, 321-333.
- [32] T. D. Schneider, R. M. Stephens, *Nucl. Acids Res.* **1990**, *25*, 6097-6100.
- [33] S. El-Gebali, J. Mistry, A. Bateman, S. R. Eddy, A. Luciani, S. C. Potter, M. Qureshi, J. L. Richardson, G. A. Salazar, A. Smart, E. L. L. Sonnhammer, L. Hirsh, L. Paladin, D. Piovesan, S. C. E. Tosatto, R. D. Finn, *Nucl. Acids Res.* **2019**, *47*, D427-D432.
- [34] G. E. Crooks, G. Hon, J. M. Chandonia, S. E. Brenner, *Genome Res.* **2004**, *14*, 1188-1190.
- [35] S. E. Calvo, C. R. Clauser, V. K. Mootha, *Nucl. Acids Res.* **2016**, *44*, D1251 - D1257.